

Dynamically entangled oscillating state in a Bose gas with an attractive polaron

Saptarshi Majumdar and Aleksandra Petković

Univ Toulouse, CNRS, Laboratoire de Physique Théorique, Toulouse, France

(Dated: February 10, 2026)

We study the out-of-equilibrium dynamics of an attractively interacting impurity suddenly immersed with a nonzero initial velocity into a system of one-dimensional weakly interacting homogeneous bosons. We uncover and characterize different dynamical regimes in the parameter space. Especially interesting is the relaxation of a fast impurity with a mass close to or exceeding the critical one, where the impurity exhibits undamped temporal long-lived velocity oscillations before reaching a stationary state. The underlying mechanism is the transient localization of a boson depletion cloud near the impurity, that oscillates around the boson density peak situated at the impurity position. The lifetime of this entangled oscillating state increases with the absolute value of the impurity-boson coupling. Cold atomic gases provide an ideal playground where this phenomenon can be probed.

I. INTRODUCTION

The motion of a distinguishable particle (an impurity) coupled to an environment is ubiquitous in physics. It describes many different fundamental phenomena [1–3]. A famous example is the notion of a polaron quasiparticle, introduced by Landau and Pekar [4], who considered the motion of an electron in a dielectric crystal. The surrounding ions try to screen the electron charge, and severely modify the properties of the bare electron, which, together with a local phonon cloud, forms a polaron [5]. The concept of polaron is nowadays broader and describes a mobile impurity dressed with a cloud of excitations of the host system.

Understanding the out-of-equilibrium dynamics of a mobile impurity in a many-body environment is a challenging problem. Particularly interesting are one-dimensional (1d) systems, where interactions can lead to very different physical phenomena with respect to their higher-dimensional counterparts [6]. In this work, we consider a 1d system of bosons. The interplay of the impurity-boson and the boson-boson interaction in out-of-equilibrium conditions leads to interesting dynamical phenomena [7–25]. While the process of the Bose polaron formation in 1d geometry has been intensively investigated in the case of repulsive impurity-boson interaction [7, 9, 10, 13, 17, 20, 22, 23, 26], this problem remains much less studied for an attractive impurity-boson interaction [25, 27].

In this work, we study the nonequilibrium dynamics of dressing and relaxation of an attractively interacting impurity suddenly immersed in the ground state of homogeneous bosons with a nonzero initial velocity. We take advantage of weak interaction between the bosons and solve the time-dependent mean-field equation of motion for bosons in the reference frame co-moving with the impurity. We investigate the dynamical response of the bosons by monitoring the time evolution of their density and phase profile. It allows us to characterize the excitations emitted in the process of energy and momentum transfer from the impurity to the bath. Apart from the peak in the boson density at the impurity position, dispersive density shock waves and a depletion cloud also form, and in a general case, they move away from the impurity leading to a locally established stationary state. We study the evolution of the impurity velocity in time, as a function of

the impurity mass, the initial velocity and the impurity-boson interaction strength.

The relaxation of a fast impurity with the mass close to or greater than the critical one is particularly interesting. After a rapid drop of the impurity velocity, a dynamically entangled state of surrounding bosons and the impurity is formed, leading to undamped temporal long-lived impurity velocity oscillations. This phenomenon is due to the trapping of the boson depletion cloud and its oscillations around the peak in the boson density situated at the impurity position. In this process, the depletion cloud gets progressively split into two parts positioned on the opposite sides of the impurity. The two depletion holes get repelled, and move away from the impurity, while the density peak continues the motion together with the impurity with a stationary velocity. The stronger the impurity-boson interaction is, the longer the lifetime of this entangled state is. Cold atoms provide an excellent platform to probe the aforementioned phenomena [28–33].

The paper is organized as follows. We introduce the model in Sec. II, and provide an analytic solution for a finite-momentum ground state of the system, and its properties in Sec. III. Section IV studies the relaxation dynamics of the system after the impurity injection into the bosonic bath, focusing on the influence of the initial impurity momentum, the impurity mass and the impurity-bath coupling. We then report and characterize a special type of dynamics of fast and sufficiently heavy impurities in Sec. V, where the impurity undergoes undamped long-lived oscillations before reaching a stationary state. The main conclusions are presented in Sec. VI.

II. MODEL

We study a system consisting of a single impurity immersed into a bath of 1d bosons at zero temperature. The system is modelled by the Hamiltonian

$$\hat{H} = \frac{\hat{P}^2}{2M} + \hat{H}_b + G\hat{\Psi}^\dagger(\hat{X})\hat{\Psi}(\hat{X}). \quad (1)$$

The impurity has a mass M . Its momentum and position operators are denoted by \hat{P} and \hat{X} , respectively. The Hamiltonian

\hat{H}_b describes interacting bosons and takes the form

$$\hat{H}_b = \int dx \left[-\hat{\Psi}^\dagger(x) \frac{\hbar^2 \partial_x^2}{2m} \hat{\Psi}(x) + \frac{g}{2} \hat{\Psi}^\dagger(x) \hat{\Psi}^\dagger(x) \hat{\Psi}(x) \hat{\Psi}(x) \right]. \quad (2)$$

The single-particle bosonic operators $\hat{\Psi}^\dagger(x)$ and $\hat{\Psi}(x)$ obey the commutation relation $[\hat{\Psi}(x), \hat{\Psi}^\dagger(x')] = \delta(x - x')$. The repulsion strength between the bosons is g . We introduce the dimensionless parameter $\gamma = mg/\hbar^2 n_0$, where m is the mass of bosons and n_0 is their mean density. The last term in Eq. (1) models the impurity-boson interaction, where the impurity couples locally to the boson density with a coupling constant G . We assume that the impurity-boson interaction is attractive, $G < 0$.

We perform the Lee-Low-Pines transformation [34] $\hat{\mathcal{H}} = \hat{U}^\dagger \hat{H} \hat{U}$, where $\hat{U} = e^{-i\hat{X}\hat{p}_b/\hbar}$ and the momentum of the bosons is $\hat{p}_b = -i\hbar \int dx \hat{\Psi}^\dagger(x) \partial_x \hat{\Psi}(x)$. In the new referent system the impurity is situated at the origin and the Hamiltonian reads as

$$\hat{\mathcal{H}} = \hat{H}_b + \frac{(p - \hat{p}_b)^2}{2M} + G \hat{\Psi}^\dagger(0) \hat{\Psi}(0). \quad (3)$$

The total momentum of the system in the laboratory frame is denoted by p and is conserved in time. At initial time, the impurity is free and has a moment $p = MV_0$, while the bosons are in their zero-momentum ground state. Then, the impurity-boson interaction is turned on, and we study the time-evolution from this far-from-equilibrium initial state.

In the following, we consider weakly-interacting bosons with $\gamma \ll 1$. In this limit, we employ the small- γ expansion of the single-particle bosonic operator [35–37]. In the leading order, one obtains the equation of motion for the condensate wave function Ψ_0 [20, 22, 38]

$$i\hbar \partial_t \Psi_0(x, t) = \left[-\frac{\hbar^2}{2} \left(\frac{1}{m} + \frac{1}{M} \right) \partial_x^2 + g |\Psi_0(x, t)|^2 + G \delta(x) + i\hbar V(t) \partial_x \right] \Psi_0(x, t). \quad (4)$$

Here, the impurity velocity V takes the form

$$V(t) = \frac{p}{M} + i \frac{\hbar}{M} \int dx \Psi_0^*(x, t) \partial_x \Psi_0(x, t). \quad (5)$$

III. FINITE-MOMENTUM ATTRACTIVE POLARON

In this section, we consider a stationary solution of Eq. (4) subject to periodic boundary conditions. It gives the stationary state reached by the system in the protocol where the boson-impurity interaction is switched on adiabatically slowly. The solution can be written as [35] $\Psi_0(x, t) = \Psi_0(x) e^{-i\mu t/\hbar}$, where μ denotes the chemical potential of bosons. In the stationary state, the impurity velocity is constant, $V(t) = V_f$.

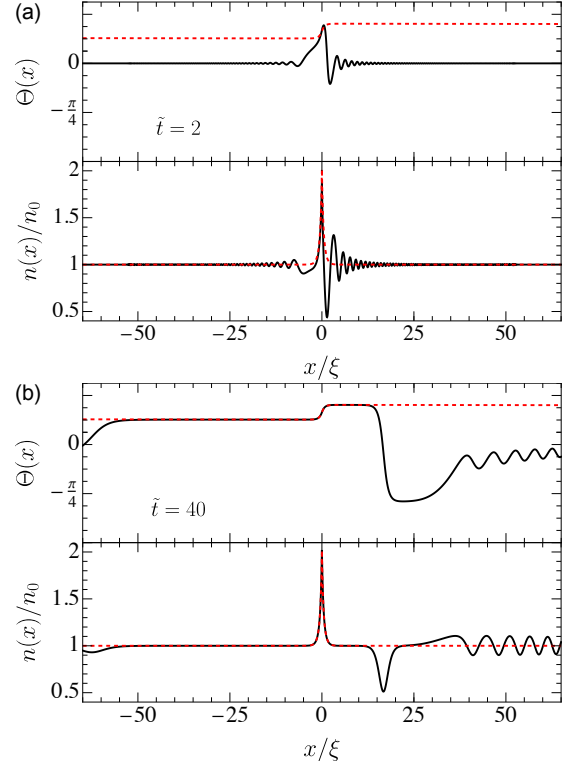


FIG. 1. Time evolution of the phase $\Theta(x, t)$ and the density $n(x, t) = |\Psi_0(x, t)|^2$ of bosons after a quench of the impurity-boson interaction, for $\tilde{G} = -0.8$, $M = 3m$, and $V_0 = 1.5v$ at (a) $\tilde{t} = tgn_0/\hbar = 2$ and (b) $\tilde{t} = 40$. The red dashed lines denote the phase and the density of the ground state (6) for the numerically obtained final impurity velocity $V_f = 0.43v$. The corresponding impurity velocity evolution in time is shown in Fig. 4a.

The solution can be evaluated analytically by a simple generalization of the result of Ref. [39]. It reads as

$$\Psi_0(x) = \sqrt{\frac{\mu}{g}} \exp \left[i \operatorname{sgn}(x) \arctan \left(\frac{b \tanh x_0}{a} \right) + i\theta \frac{x}{L} \right] \times \left[a - i b \operatorname{sgn}(x) \tanh \left(\frac{b|x|}{\xi \sqrt{1+m/M}} + x_0 \right) \right] \quad (6)$$

in the thermodynamic limit, for the total momentum of the system being in the interval $-\pi\hbar n_0 < p \leq \pi\hbar n_0$. Here the system length is L , the healing length is $\xi = \hbar/\sqrt{m\mu}$, and the sound velocity is $v = \sqrt{\mu/m}$. Additionally, $a = V_f/v\sqrt{1+m/M}$ and $b = \sqrt{1-a^2}$. The term containing $\delta(x)$ in Eq. (4) imposes the jump of the first spatial derivative of the wave function at the origin. From this constraint, it follows that the shift parameter x_0 satisfies

$$\frac{G}{\hbar v} \frac{1}{\sqrt{1+m/M}} (a^2 + b^2 \tanh^2 x_0) = b^3 \tanh x_0 \operatorname{sech}^2 x_0. \quad (7)$$

Apart from the boson density, the impurity also modifies the phase of the condensate, causing a phase drop θ across its

position. In the thermodynamic limit, θ reads as

$$\theta = 2 \arctan \left(\frac{b}{a} \right) - 2 \arctan \left(\frac{b}{a} \tanh x_0 \right). \quad (8)$$

Thus, the contribution $\theta x/L$ in the phase of the condensate wave function (6), takes care about periodic boundary conditions. Note that this term gives a contribution to the system momentum carried by the supercurrents, but does not contribute to the energy.

Equation (7) admits solutions only for the impurity velocities smaller than the critical velocity, $|V_f| \leq v_c$. Contrary to the case of a repulsively interacting impurity [39], the critical velocity does not depend on $\tilde{G} = G/\hbar v$ here and reads as $v_c = v\sqrt{1+m/M}$. Moreover, for $\tilde{G} < 0$, there is just *one* physical solution of Eq. (7) that leads to an increase of the boson density at the impurity position. This solution for x_0 is a complex number and satisfies $\tanh x_0 > 1$, with the imaginary part of x_0 being $i\pi/2$. Then, $\tanh(\beta|x| + x_0) = \coth[\beta|x| + \text{Re}(x_0)]$ where β is a real number. Thus, the stationary solution (6) describes a peak in the boson density centred at the impurity position. Contrary to the repulsive case, the phase drop θ is negative for $V_f > 0$, implying the phase increase across the impurity position. The phase and the density of bosons are shown by the red dashed line in Fig. 1.

We consider a finite impurity coupling constant \tilde{G} . The chemical potential is calculated from the constraint $\int_{-L/2}^{L/2} dx |\Psi_0(x)|^2 = n_0 L$, and it takes the following form

$$\mu = gn_0 + 2b\hbar \frac{1 - \tanh x_0}{L} \sqrt{\frac{gn_0}{m}(1 + m/M)}. \quad (9)$$

Here b and x_0 are evaluated by replacing μ by its leading order term $\mu_0 = gn_0$. We are not interested in finite size corrections. Thus, from now on, all the parameters will be evaluated using μ_0 instead of μ , if not stated differently. We have evaluated the first finite-size correction in μ because it is needed for the subsequent evaluation of the energy in the thermodynamic limit.

Using Eq. (5), we obtain the relation between the initial impurity momentum $p = MV_0$ and its final value MV_f , that reads as

$$p = MV_f - 2\hbar n_0 ab (1 - \tanh x_0) + \hbar n_0 \theta + 2k\pi\hbar n_0, \quad (10)$$

for $\pi\hbar n_0(2k - 1) < p \leq \pi\hbar n_0(2k + 1)$. Here k is an integer. Note that increasing V_f from zero to v_c , the density peak at the impurity position increases, as well as the absolute value of the phase drop across the impurity. We emphasize that V_f satisfying Eq. (10) is not the final impurity velocity for the post-quench dynamics, as will be shown in Sec. IV. Equation (10) describes the case where the impurity-boson interaction is switched on adiabatically slowly such that no excitations are generated.

We define the energy E_p of the impurity dressed by the cloud of bosons as a difference of the ground state energy of the Hamiltonian (3) at a given total momentum p and its ground state energy at zero momentum in the absence of the

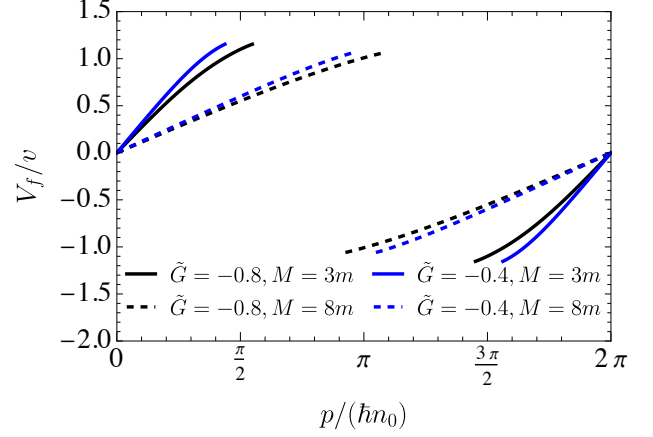


FIG. 2. Final impurity velocity (10) of the ground state (6) as a function of the system momentum for different impurity masses and coupling constants. Here $\gamma = 0.1$.

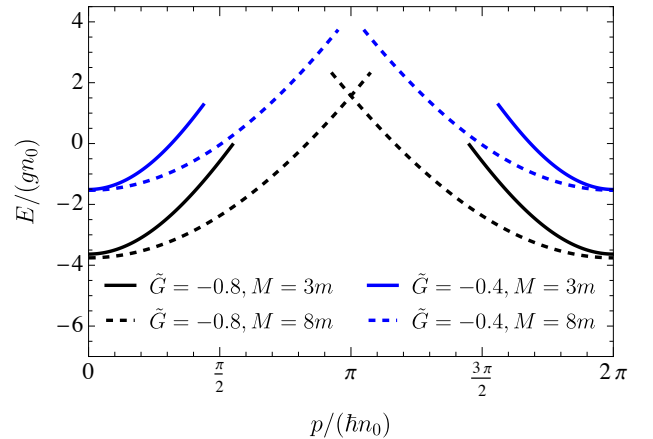


FIG. 3. Ground-state energy dispersion (11) for two different values of \tilde{G} and M/m at $\gamma = 0.1$. Here, $M = 8m > M_c$ for $\tilde{G} = -0.8$.

impurity. We evaluate the polaron energy E_p to be

$$\begin{aligned} \frac{E_p}{gn_0} = & \frac{2}{3} b^3 \frac{\sqrt{1+m/M}}{\sqrt{\gamma}} [1 - \tanh^3(x_0)] + \frac{MV_f^2}{2gn_0} \\ & + \frac{1}{3} b^3 \frac{\sqrt{1+m/M}}{\sqrt{\gamma}} [\tanh^3(x_0) - 3\tanh(x_0) + 2], \end{aligned} \quad (11)$$

as in the case of a repulsively interacting impurity [3, 23]. Here V_f satisfies Eq. (10) and x_0 obeys Eq. (7). Using the path-integral approach, the energy dispersion has been evaluated in Ref. [40] in a somewhat cumbersome integral form. Evaluating the latter, we have verified that it gives the polaron energy in agreement with Eq. (11). From Eq. (10) follows that changing the momentum as $p \rightarrow p \pm 2\pi\hbar n_0$, V_f and x_0 remain unaltered. As a result, the energy (11) is a periodic function of momentum, with the period $2\pi\hbar n_0$.

Figures 2 and 3 show the final impurity velocity (10) and the energy dispersion (11) as a function of the total system

momentum, respectively, for different coupling constants \tilde{G} and impurity masses. Contrary to the repulsive case [23], the wave function (6) provides the ground-state solution only in a certain interval of momenta. The latter is given by Eq. (10), where the final velocity takes values in the interval $(-v_c, v_c)$. The reason for the existence of forbidden momenta is the absence of a second physical solution of Eq. (7) for a given $V_f < v_c$. However, we will show in Sec. IV that the boson density profile around the impurity in a stationary state obtained after a quench of the impurity-boson interaction, for an arbitrary system momentum, is given by Eq. (6), but with a final velocity V_f that does not satisfy Eq. (10). The reason for the latter is the emission of additional excitations in the form of dispersive shock waves and solitons.

Increasing the impurity mass or its coupling constant, the range of momenta where the analytic solution (6) exists increases, and the two energy branches approach each other, see Fig. 3. Thus, as for a repulsive impurity potential [41, 42], one can define the critical mass M_c when the two energy branches touch each other. As a result, the cusps appear in the ground-state energy at momenta $p = (2m+1)\pi\hbar n_0$, with m being an integer. Then, Eq. (6) is the ground state at all momenta. For $M > M_c$, the energy branches cross each other leading to a rich energy landscape.

Note that in the case of a strong attractive coupling, $|\tilde{G}| \gg 1$, the number of bosons gathered around the impurity is negligible with respect to the number of bosons in the remaining part of the system as long as $|\tilde{G}| \ll L\sqrt{mgn_0}/\hbar$. This inequality gives also the condition under which the expansion (9) is valid. However, the density at the impurity position grows with \tilde{G} as $n(0) = n_0\tilde{G}^2/(1+m/M)$, and the polaron energy (11) behaves as $E_p \propto \tilde{G}^3gn_0$. It is expected that a modeling of the impurity-boson interaction with a finite-range potential instead of the contact one will cure this problem [43]. Namely, it was shown that a finite-range impurity potential leads to a finite zero-momentum polaron energy in the strong coupling limit [43]. Also, at strong coupling, a limited number of potentially bound bosons [18, 44, 45] may become relevant. In the following sections, the phenomena we are interested in do not require a strong coupling, and we consider a weak to moderate coupling constant \tilde{G} .

IV. POST-QUENCH DYNAMICS OF POLARON FORMATION AND RELAXATION

In this section, we study the system time evolution after a sudden injection of a finite-momentum impurity into the background bosons. At initial time the impurity is free, while the bosons are in their zero-momentum ground state $\Psi_0(x, 0) = \sqrt{n_0}$. We solve numerically the time-dependent Gross-Pitaevskii like equation (4) with periodic boundary conditions by implementing a conservative finite-difference scheme in a fully implicit manner [46]. A first-order upwind scheme [47] is used in the discretization of the drift term. The obtained system of non-linear equations is solved in an iterative fashion [46]. The system size is taken to be sufficiently long, such that the emitted density waves do not reach the

boundaries of the system during the reported relaxation.

After the immersion, the impurity slows down on the time-scale of several \hbar/gn_0 , as shown in Fig. 4a. The higher the initial velocity is, the longer the impurity relaxation time is. The impurity transfers a part of its momentum to the bosonic bath by triggering the emission of dispersive density shock waves [48, 49], see Fig. 1a. Due to the attractive nature of the impurity-bath interaction, the bosons near the impurity gather around it forming a peak in the density. For a sufficiently high initial impurity velocity, a depletion hole separates from the density shock wave, taking the form of a gray soliton, as illustrated in Fig. 1b. As time progresses, the shock-wave fronts and the soliton move away from the impurity location, the impurity velocity reaches a final stationary value smaller than the critical velocity and locally the ground state (6) is established. As a hallmark of the zero temperature bath superfluidity, the impurity final velocity is nonzero in a general case.

We emphasize that Eq. (6), for a numerically obtained V_f , describes the boson density peak around the impurity in obtained stationary states for *all* values of the initial impurity momentum $p = MV_0$, including the forbidden momentum sector. The latter is given by values of p different from those obtained by Eq. (10) with V_f satisfying $|V_f| \leq v_c$. However, the final impurity velocity is not given by Eq. (10), see Fig. 4b, since some momentum is transmitted to the density waves and the soliton, and these excitations are not taken into account by the analytic solution (6). Equation (10) is valid in the case where the impurity-boson interaction is turned on adiabatically slowly such that no excitations are generated.

Increasing the initial impurity velocity V_0 above some threshold, the final velocity decays and more energetic solitons are emitted, as illustrated in Fig. 4. As a result, the maximal soliton depletion increases with V_0 . However, both the soliton depth and the final impurity velocity show a tendency of smooth saturation into a constant value for a sufficiently high V_0 . As a result, the system remains locally in the same stationary state as V_0 is further increased, while the energy and momentum carried by the dispersive shock waves increase. A similar dynamical crossover was reported for a repulsive impurity-boson interaction [23].

For stronger impurity-bath coupling, the deviation between numerically obtained values of V_f and those following from Eq. (10) becomes more pronounced even at low p , due to the emission of bigger-amplitude shock waves, see Fig. 4b. For the case of $\tilde{G} = -2$ and $M = 3m$ shown in Fig. 4b, for $V_0 > 2.5v$, the impurity dynamics changes drastically and a new dynamical regime occurs, which will be discussed in Sec. V. There, the impurity exhibits transient temporal velocity oscillations before reaching the stationary state (6).

The impurity time evolution as a function of the dimensionless impurity coupling constant \tilde{G} is shown in Fig. 5 for $M = 3m$ and $V_0 = 2.5v$. The impurity relaxation time decreases as \tilde{G} increases. In the parameter region shown in Fig. 5, the final impurity velocity also decreases with \tilde{G} , and finally, for a very strong coupling, the impurity changes the direction of motion with respect to the initial one.

We study the relaxation dynamics for different values of the impurity mass $M < M_c$ in Fig. 6, while keeping other param-

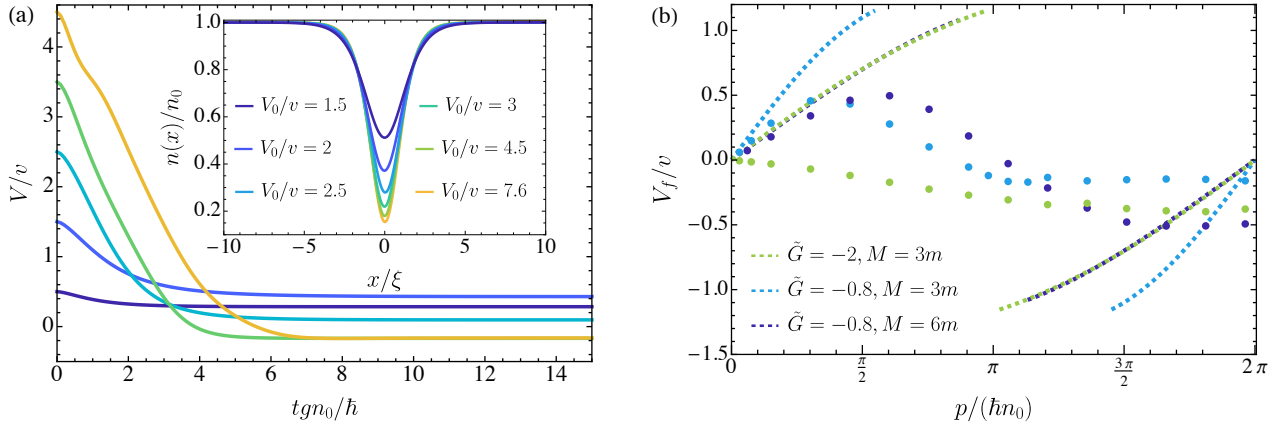


FIG. 4. (a) Time-evolution of the impurity velocity for $M = 3m$ and $\tilde{G} = -0.8$ for different initial velocities. Here $\gamma = 0.1$. (inset) The density profile of emitted soliton for different initial impurity velocities V_0 for the aforementioned parameters. (b) Final impurity velocity V_f as a function of the initial impurity momentum $p = MV_0$ for three different sets of parameters. Here, the dotted lines denote the analytic expression (10), while the points denote the numerically obtained values of V_f . One can express $p/\hbar n_0 = (V_0/v)(M\sqrt{\gamma}/m)$.

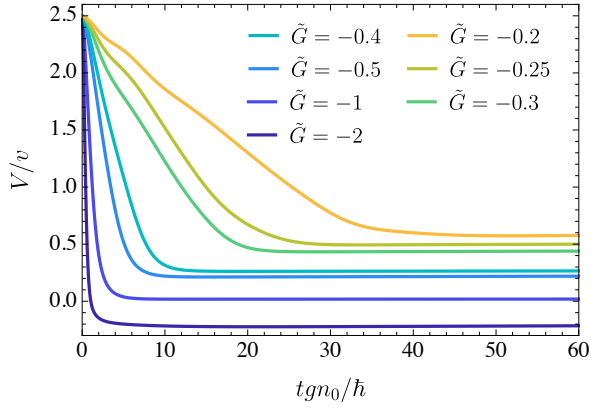


FIG. 5. Time evolution of the impurity velocity for $M = 3m$ and $V_0 = 2.5v$ for different dimensionless impurity-bath coupling \tilde{G} . Here $\gamma = 0.1$.

eters fixed, $\tilde{G} = -0.2$ and $V_0 = 2.5v$. For heavier impurities, the deceleration is slower, leading to a longer relaxation time. For considered parameters, Fig. 6 shows the final impurity velocity that decreases with M . As a result, the energy transferred to the bath increases with M , and the emitted solitons become more energetic. Sufficiently heavy impurity changes the initial direction of motion, reaching a negative final velocity. Carefully looking at Fig. 4b, one sees that the final velocity can also become higher by increasing the ratio M/m for the same initial velocity and \tilde{G} , see $V_0 = \pi v/(10\sqrt{\gamma})$ ($p = 3\pi\hbar n_0/10$ for $M = 3m$). The reason is the nonmonotonic dependence of V_f on V_0 .

Note that Eq. (4) gives the modified sound velocity $v\sqrt{1+m/M}$. Although all the obtained final velocities are smaller than the critical velocity v_c , a light impurity can have the final velocity bigger than the sound velocity v , since $V_f \leq v_c = v\sqrt{1+m/M}$, see Fig. 6. This problem does not arise if the $1/M$ contribution in the first term in Eq. (4) is

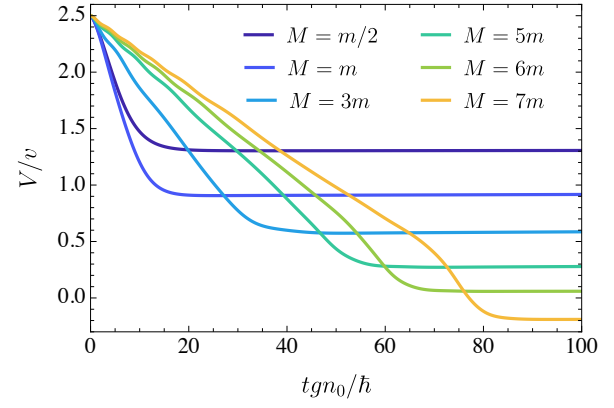


FIG. 6. Time evolution of the impurity velocity for $\tilde{G} = -0.2$ and $V_0 = 2.5v$ for different impurity masses. Here $\gamma = 0.1$.

absent [23]. To characterize the ground state obtained for this alternative equation of motion, one should replace $1+m/M$ by 1 in all the equations in Sec. III. The differences between the two approaches are thus expected to be visible for not too heavy impurity. Using the alternative equation of motion, we examine the post-quench dynamics in Fig. 7 and compare it to the previously obtained results shown in Fig. 4a. Now, the impurity relaxation towards a stationary state becomes faster, and the obtained final velocities differ. In the regime where V_f saturates, the differences in V_f become smaller.

V. ENTANGLED OSCILLATING STATE

A. Physical mechanism

In this section, we study the out-of-equilibrium dynamics of a fast impurity with a mass greater than or close to the critical one, where a novel dynamical regime takes place. The latter is

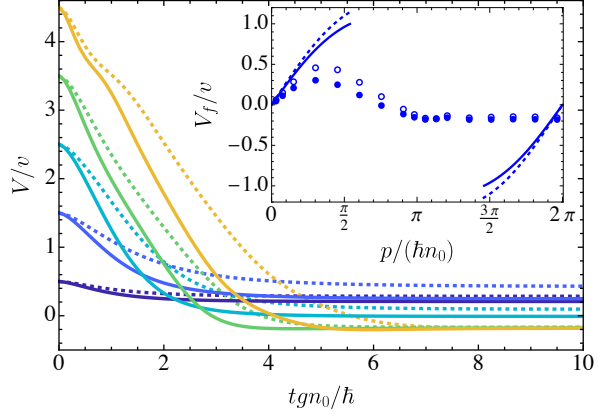


FIG. 7. Impurity velocity as a function of time for $\tilde{G} = -0.8$, $M = 3m$, $\gamma = 0.1$ for different initial velocities, obtained using Eq. (4) (the dashed line) and the alternative equation of motion (the solid line). The inset shows the final impurity velocity as a function of initial impurity momentum for the same parameters. The lines and the circles represent the analytical prediction in the case of the adiabatic turning-on of the impurity-boson interaction (the dashed and the solid line show the Eq. (10) and its modified version for the alternative equation of motion, respectively) and the numerically obtained values (the hollow circles for the standard and the filled ones for the alternative equation), respectively.

illustrated in Fig. 8a for $\tilde{G} = -0.8$, $M = 9m$, and $V_0 = 2v$. After a rapid drop, the impurity velocity exhibits undamped long-lived oscillations in time, before reaching a stationary state.

In order to explain the underlying mechanism, we study the accompanying time evolution of the boson density in the vicinity of the impurity in Fig. 8b. Note that the force exerted by the bosons on the impurity is given by the gradient of the potential, and reads as

$$F(t) = \int dx \Psi_0^*(x, t) \partial_x [G\delta(x)] \Psi_0(x, t) \\ = -\frac{G}{2} [\partial_x n(x, t)|_{x=0^-} + \partial_x n(x, t)|_{x=0^+}]. \quad (12)$$

In Fig. 8b, the red solid and blue dashed arrows denote the vectors of the dimensionless impurity velocity V/v and the dimensionless force, $F/(gn_0^2)$, acting on the impurity, respectively. After the injection into the condensate, the impurity decelerates rapidly while emitting dispersive density shock waves, as in a general case studied in Sec. IV. Meanwhile, the boson density peak builds up at the impurity position. The impurity slows down and reaches zero velocity. The density profile close to this time, shown in Fig. 8b at $\tilde{t} = tgn_0/\hbar = 5$, reveals that the heavy and fast impurity has created an almost complete depletion in front of it. The interference between the density peak and this depletion area makes the peak nearly invisible. As time passes, the shock wave moves away from the impurity. In contrast to the scenario of Sec. IV, the depletion cloud here does not separate from the impurity, and instead forms an entangled state with the density peak and the impurity. The steep boson density slope caused by the depletion

that remains attached to the impurity, in front of it, results in a negative force (12) acting on the impurity. Thus, the impurity changes the direction of motion and accelerates, building up the density peak at its position, as well as a new depletion hole positioned in front of it, as shown at $\tilde{t} = 6.5$. Simultaneously, the previous depletion cloud, now situated behind the impurity, diminishes. As a result, the magnitude of the force $|F(t)|$ decays. The impurity reaches its maximal negative velocity and the slope of the density profile becomes symmetric around the impurity, leading to a vanishing friction force, see the density profile at $\tilde{t} = 7.5$ that is close to this characteristic time. Afterwards, the depletion hole in front of the impurity continues to grow, while the one behind it diminishes further, as shown at $\tilde{t} = 8.5$. As a result of this asymmetry in the boson density, the friction force changes its direction and the impurity slows down, resulting in a less pronounced density peak. The increasing boson density asymmetry leads to a continuous increase of the friction force in time. The latter reaches its maximal value, while the impurity velocity arrives at zero value, see Fig. 8b at $\tilde{t} = 10$. The impurity again changes its direction of motion, and this process repeats. However, the magnitude of the maximal positive impurity velocity exceeds the maximal negative one, and the density shows a more prominent peak at the impurity position at $\tilde{t} = 12.5$, 15 and 18.5. The above described process can be understood as a collision of the depletion cloud and the peak, where the latter gets trapped and oscillates inside the depletion hole.

The evolution of the impurity momentum $p_i(t) = MV(t)$ and the momentum of bosons situated around the impurity $p_b(t) = -i\hbar \int_{-W}^W dx \Psi_0^*(x, t) \partial_x \Psi_0(x, t)$ is shown in Fig. 9. Here, the half-width of the interval is $W = 15\xi$, such that it encompasses the impurity and the depletion hole during the oscillations. The momenta of the impurity and the neighbouring bosons have opposite signs and oscillate in anti-phase. The total momentum, $p_b + p_i$, also exhibits oscillations, but with a very small amplitude. Moreover, the maximum of the boson density peak is always situated at the impurity position and does not oscillate around it. Note that the oscillations trigger emission of density waves propagating in the remaining part of the system, resulting in a decrease of the energy of the subsystem composed of the impurity and the surrounding bosons.

Each time the system passes through the state with the maximal impurity velocity, the two depletion clouds positioned on the opposite sides of the impurity become more separated from the impurity, and thus less influencing the density profile at the impurity position and the resulting force. As a result, the density peak realized in this state grows in time, as shown in the inset of Fig. 8a. Moreover, the friction force remains approximately zero for a longer time during which the system stays in this maximal- V state. Finally, the repulsion between the depletion clouds and the impurity and the depletion-depletion repulsion win and the two depletion holes separate and move away from the impurity in the opposite directions, taking the form of grey solitons. As a result, the stationary configuration (6) is realised locally, and the density peak moves together with the impurity. The final impurity velocity is close to the maximal positive velocity of intermediate

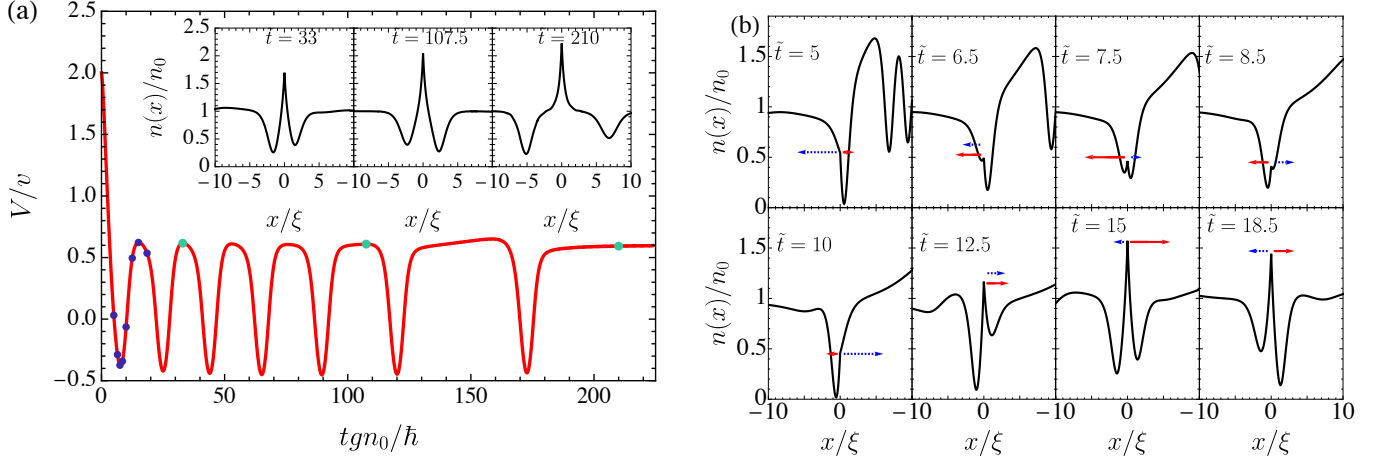


FIG. 8. (a) Impurity velocity as a function of time for $\tilde{G} = -0.8$, $M = 9m$, $\gamma = 0.1$, and $V_0 = 2v$. The inset shows the boson density in the frame co-moving with the impurity at different times, marked with light green points in the velocity time dependence. In the inset, the x axis represents the dimensionless length x/ξ , and the dimensionless time is defined as $\tilde{t} = tgn_0/\hbar$. (b) Boson density $n(x)/n_0$ in the frame co-moving with the impurity for the aforementioned parameters shown over one period of oscillations at the time-points marked by dark blue points on the velocity curve in (a). The red solid and the blue dashed arrows denote the direction of the dimensionless impurity velocity V/v and the dimensionless force acting on the impurity $F/(gn_0^2)$ at the specific timeframes in the laboratory frame, respectively. The lengths of the arrows are proportional to their magnitudes.

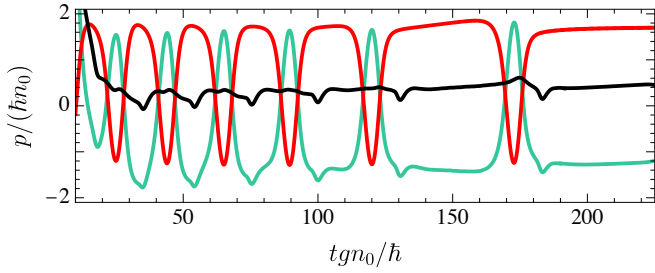


FIG. 9. Momentum of bosons p_b situated in the vicinity of the impurity in the interval $x \in (-15\xi, 15\xi)$ and the impurity momentum p_i are shown by the light green and the red line, respectively. The black line represents $p_b + p_i$. Here $\tilde{G} = -0.8$, $M = 9m$, $V_0 = 2v$, and $\gamma = 0.1$.

time oscillations.

B. Dependence on the initial impurity velocity

The effect of the initial impurity velocity V_0 on the dynamics and the entangled-state formation is illustrated in Fig. 10a. The time evolution of the impurity velocity for different values of V_0 is shown for $\tilde{G} = -0.8$, $M = 8m$ and $\gamma = 0.1$. For $V_0 \leq 1.8v$, the impurity relaxes to a stationary state in a standard manner, as described in Sec. IV. For $V_0 = 2v$, the oscillating state characterized in Sec. VA is realized. In this instance, however, the velocity oscillations are symmetric around $V = 0$, such that $V_{\max} \approx -V_{\min}$. At higher initial impurity velocity, we see another aspect of this phenomenon where the system enters into oscillations while the density peak at the impurity position is not fully formed. While this

trend was also present for the parameters of Fig. 8, the effect is significantly more pronounced for the current parameters. As a result, the impurity velocity exhibits a progressive increase of the oscillation amplitude in time, while the density peak forms as it oscillates. These oscillations then stabilize, i.e., the oscillation amplitude becomes constant, before reaching a stationary case. This dynamical regime is shown in Fig. 10a for $V_0 = 2.35v$ and $V_0 = 2.5v$. Moreover, Fig. 10a suggests that the oscillation frequency increases as V_0 is increased.

C. Dependence on the strength of the impurity coupling

Next, we examine the influence of \tilde{G} on the entangled state. Figure 10b shows the impurity velocity time evolution for different values of \tilde{G} for $M = 8m$ and $V_0 = 2v$. At $\tilde{G} = -0.4$, the impurity does not exhibit the velocity oscillations for the aforementioned parameters. In this case, the impurity mass is below, but in the close vicinity of the critical mass. The shock wave and the complete depletion cloud are formed at $\tilde{t} = 5$, while only a partially formed density peak gets captured inside the depletion cloud till $\tilde{t} = 30$. Then the depletion gets split into two parts that move away from the impurity. Increasing \tilde{G} , the process of the peak formation is more rapid, and the impurity enters into the oscillating state. By making the impurity-bath coupling more attractive, the absolute value of the force acting on the impurity increases, $F \sim G$, leading to a higher-frequency and smaller-amplitude velocity oscillations. For the parameters shown in Figure 10b, the oscillations remain symmetric around $V = 0$, with $V_{\min} \approx -V_{\max}$. The amplitude of density waves triggered by the impurity oscillations increases with the absolute value of the impurity-bath coupling, leading to a bigger rate of energy decrease of the subsystem consisting of the combined structure of the density

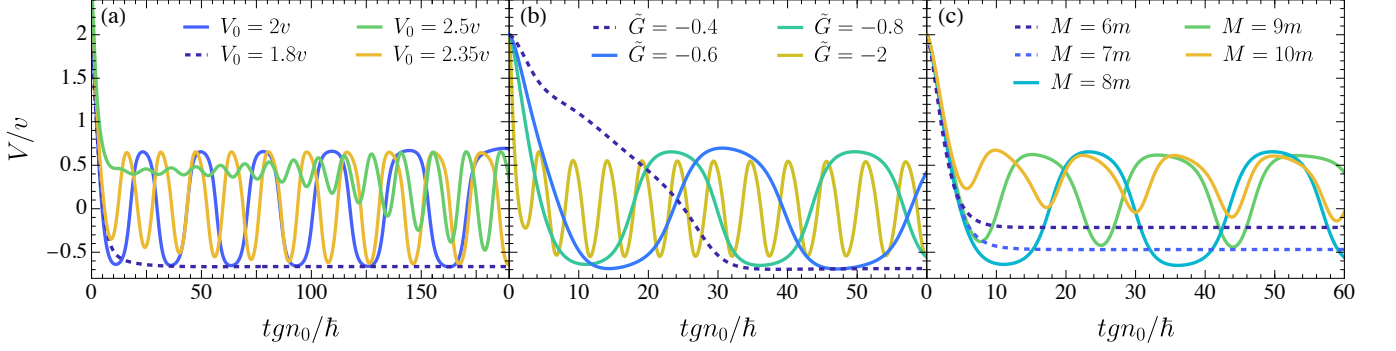


FIG. 10. Impurity velocity as a function of time (a) for $\tilde{G} = -0.8$ and $M = 8m$ for different values of the initial impurity velocity, (b) for $M = 8m$ and $V_0 = 2v$ for different impurity-bath coupling \tilde{G} , and (c) for $\tilde{G} = -0.8$ and $V_0 = 2v$ for different impurity masses. At all figures $\gamma = 0.1$.

peak with the depletion holes and the impurity. We stress that the lifetime of the entangled state increases by increasing $|\tilde{G}|$. For example, a change of \tilde{G} from -0.6 to -0.8 leads to an approximately 65% longer lifetime.

D. Dependence on the impurity mass

The effect of the impurity mass M on the oscillations is shown in Fig. 10c for $\tilde{G} = -0.8$ and $V_0 = 2v$. For lighter impurities, $M = 6m$ and $7m$, the oscillations are absent and the system follows the scenario of Sec. IV. Note that these values of the impurity mass are smaller than M_c . Increasing M , the entangled state occurs. As the impurity becomes heavier $M > 8m$, V_{\max} almost remains the same, whereas V_{\min} increases rapidly, decreasing the oscillation amplitude. This asymmetry manifests also in the boson density at minima and maxima of $V(t)$, with the boson density peak being smaller at V_{\min} than at V_{\max} . Moreover, the maximal value of the force (12) felt by the impurity increases slightly with M . However, the amplitude of the impurity velocity oscillations decreases rapidly with M , thus leading to an increase of the oscillation frequency.

For $M = 10m$, the oscillation amplitude increases in time in the initial stage of the oscillations because the peak in the boson density at the impurity position is still forming. A heavier impurity produces also more important density waves during oscillations, resulting in a higher rate of energy decay of the subsystem composed of the boson density peak, the impurity and the depletion cloud. Finally, note that the lifetime of the entangled state formed at $M = 8m$ is approximately 90% longer than for $M = 9m$. The latter is shown in Fig. 8a.

We stress that the entangled state can also be formed for an impurity lighter than the critical one. For example, for the parameters of Fig. 10c, the impurity with a mass $M = 7m < M_c$ does not oscillate at $V_0 = 2$, but increasing its initial velocity to $V_0 = 2.5$ the above described entangled state is realised. Another example is a moderate \tilde{G} , e.g., with $\tilde{G} = -2$, $M = 3m < M_c$, $V_0 \geq 3v$ and $\gamma = 0.1$. The dynamics for $V_0 = 3.5v$ is shown in Fig. 11. Here, the shape of the oscillations is quite different. However, the underlying mech-

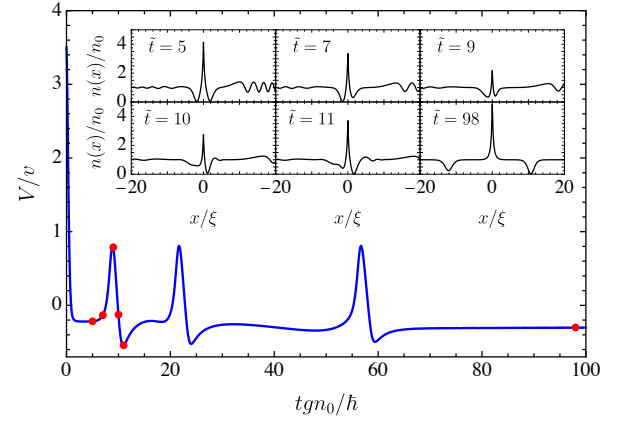


FIG. 11. Time evolution of the impurity velocity for $M = 3m$, $V_0 = 3.5v$ and $\tilde{G} = -2$. Here $\gamma = 0.1$. The inset shows the time evolution of the boson density around the impurity.

anism is the same, the transient localization of the depletion hole around the impurity position, as illustrated in the inset of Fig. 11. In Fig. 4b, we present the final velocity as a function of the initial one. We observe that the lifetime of the entangled state is a non-monotonic function of V_0 for these parameters.

E. Repulsively interacting impurity

Here, we make a comparison with the relaxation of a repulsively interacting impurity in a system of 1d bosons. In the case of both strongly interacting bosons and the impurity, an initially fast impurity exhibits slowly decaying oscillations in time before reaching a stationary state [9, 10]. This phenomenon was dubbed quantum flutter. It was claimed that quantum flutter cannot be captured by a hydrodynamic theory and the Gross-Pitaevskii equation, and that it requires the strong coupling regime [9]. Recently, we have shown that the description within the Gross-Pitaevskii equation reveals the velocity oscillations of a heavy fast impurity in a system of weakly interacting bosons [23]. Moreover, the oscillations

are much more pronounced for a weakly coupled impurity.

In a system of weakly interacting bosons, contrary to the case of an attractively interacting impurity, the repulsive one exhibits a damped oscillations [23]. Furthermore, the oscillations disappear at strong \tilde{G} , in contrast to the entangled-oscillating state that gets longer-lived as $|\tilde{G}|$ is increased. The underlying mechanisms are also different. In the repulsive case, $G > 0$, an effective attractive interaction between the local depletion cloud and the impurity produces damped oscillations of the depletion cloud around the impurity until their positions coincide and they continue the motion together. For $G < 0$, the density peak does not oscillate around the impurity, and its maximal density is situated at the impurity position during the impurity velocity oscillations.

VI. CONCLUSIONS

In this work, we have studied the far-from-equilibrium dynamics of an attractively interacting impurity suddenly injected with a finite velocity into a ground state of a system of weakly-interacting homogeneous 1d bosons. We have characterized the relaxation dynamics of both the background bosons and the impurity in Sec. IV, focusing on the emitted excitations, the relevant timescales and the final impurity velocity as a function of the initial velocity, the impurity mass and the impurity-boson coupling strength. We have uncovered a novel dynamical phenomenon resulting from a fast impurity with a mass close to or greater than the critical one, see Sec. V. The impurity velocity undergoes undamped long-lived oscil-

lations in time before reaching a stationary state. The underlying physical mechanism is the formation of an entangled non-stationary state where the local boson depletion cloud gets temporarily localized and oscillates around the density peak situated at the impurity position. The interference between the depletion hole and the peak results in a force that provokes the impurity oscillations. The momenta of the impurity and the surrounding bosons oscillate in anti-phase, until the depletion cloud gets split into two parts situated on different sides of the impurity. Due to the repulsive impurity-depletion and the depletion-depletion interaction, the depletion holes liberate and move away in the opposite directions from the impurity, while locally a stationary state is reached. An increase of the initial impurity velocity, the impurity mass or the absolute value of the impurity-boson coupling is beneficial for the formation of the entangled oscillating state. These parameters also determine the amplitude, the frequency and the lifetime of the oscillations, see Sec. V. Importantly, the stronger the impurity-boson attraction is, the longer the lifetime of the entangled state is and the higher the frequency of the oscillations is. Cold atomic gases provide an ideal playground for the impurity physics [28–33], where this phenomenon should be experimentally observable.

ACKNOWLEDGMENTS

This study has been partially supported through the EUR grant NanoX n° ANR-17-EURE-0009 in the framework of the “Programme des Investissements d’Avenir”.

[1] L. D. Landau and I. M. Khalatnikov, *Zh. Eksp. Teor. Fiz.* **19**, 709 (1949).

[2] J. T. Devreese and A. S. Alexandrov, *Rep. Prog. Phys.* **72**, 066501 (2009).

[3] M. Schecter, D. Gangardt, and A. Kamenev, *Ann. Phys.* **327**, 639 (2012).

[4] L. D. Landau and S. I. Pekar, *Zh. Eksp. Teor. Fiz.* **18**, 419 (1948).

[5] H. Fröhlich, *Advances in Physics* **3**, 325 (1954).

[6] T. Giamarchi, *Quantum Physics in One Dimension* (Clarendon press, Oxford, 2003).

[7] M. B. Zvonarev, V. V. Cheianov, and T. Giamarchi, *Phys. Rev. Lett.* **99**, 240404 (2007).

[8] D. M. Gangardt and A. Kamenev, *Phys. Rev. Lett.* **102**, 070402 (2009).

[9] C. Mathy, M. Zvonarev, and E. Demler, *Nature Phys.* **8**, 881 (2012).

[10] M. Knap, C. J. M. Mathy, M. Ganahl, M. B. Zvonarev, and E. Demler, *Phys. Rev. Lett.* **112**, 015302 (2014).

[11] N. J. Robinson, J.-S. Caux, and R. M. Konik, *Phys. Rev. Lett.* **116**, 145302 (2016).

[12] Y. E. Shchadilova, R. Schmidt, F. Grusdt, and E. Demler, *Phys. Rev. Lett.* **117**, 113002 (2016).

[13] A. Lampo, S. H. Lim, M. Á. García-March, and M. Lewenstein, *Quantum* **1**, 30 (2017).

[14] O. Gamayun, O. Lychkovskiy, E. Burovski, M. Malcomson, V. V. Cheianov, and M. B. Zvonarev, *Phys. Rev. Lett.* **120**, 220605 (2018).

[15] M. Drescher, M. Salmhofer, and T. Enss, *Phys. Rev. A* **99**, 023601 (2019).

[16] O. Gamayun, O. Lychkovskiy, and M. B. Zvonarev, *SciPost Phys.* **8**, 053 (2020).

[17] S. I. Mistakidis, G. C. Katsimiga, G. M. Koutentakis, T. Busch, and P. Schmelcher, *Phys. Rev. Lett.* **122**, 183001 (2019).

[18] M. Drescher, M. Salmhofer, and T. Enss, *Phys. Rev. Res.* **2**, 032011 (2020).

[19] K. Seetharam, Y. Shchadilova, F. Grusdt, M. B. Zvonarev, and E. Demler, *Phys. Rev. Lett.* **127**, 185302 (2021).

[20] G. M. Koutentakis, S. I. Mistakidis, and P. Schmelcher, *Atoms* **10**, 3 (2022).

[21] A. Petković and Z. Ristivojevic, *Phys. Rev. Lett.* **131**, 186001 (2023).

[22] M. Will and M. Fleischhauer, *New J. Phys.* **25**, 083043 (2023).

[23] S. Majumdar and A. Petković, *Phys. Rev. A* **112**, 053326 (2025).

[24] S. Majumdar and A. Petković, *arXiv:2511.20326* (2025).

[25] P. Wysocki, M. Tylutki, and K. Jachymski, *New J. Phys.* **28**, 013201 (2026).

[26] Z.-H. Zhang, Y. Jiang, H.-Q. Lin, and X.-W. Guan, *Phys. Rev. A* **110**, 023329 (2024).

[27] S. I. Mistakidis, F. Grusdt, G. M. Koutentakis, and P. Schmelcher, *New J. Phys.* **21**, 103026 (2019).

[28] J. Catani, G. Lamporesi, D. Naik, M. Gring, M. Inguscio, F. Minardi, A. Kantian, and T. Giamarchi, *Phys. Rev. A* **85**, 023623

(2012).

[29] F. Meinert, M. Knap, E. Kirilov, K. Jag-Lauber, M. B. Zvonarev, E. Demler, and H.-C. Nägerl, *Science* **356**, 945 (2017).

[30] M.-G. Hu, M. J. Van de Graaff, D. Kedar, J. P. Corson, E. A. Cornell, and D. S. Jin, *Phys. Rev. Lett.* **117**, 055301 (2016).

[31] N. B. Jørgensen, L. Wacker, K. T. Skalmstang, M. M. Parish, J. Levinsen, R. S. Christensen, G. M. Bruun, and J. J. Arlt, *Phys. Rev. Lett.* **117**, 055302 (2016).

[32] J. Etrych, G. Martirosyan, A. Cao, C. J. Ho, Z. Hadzibabic, and C. Eigen, *Phys. Rev. X* **15**, 021070 (2025).

[33] F. Grusdt, N. Mostaan, E. Demler, and L. A. P. Ardila, *Reports on Progress in Physics* **88**, 066401 (2025).

[34] T. D. Lee, F. E. Low, and D. Pines, *Phys. Rev.* **90**, 297 (1953).

[35] L. P. Pitaevskii and S. Stringari, *Bose-Einstein Condensation*, International Series of Monographs on Physics (Oxford University Press, Oxford, New York, 2003).

[36] A. G. Sykes, M. J. Davis, and D. C. Roberts, *Phys. Rev. Lett.* **103**, 085302 (2009).

[37] B. Reichert, Z. Ristivojevic, and A. Petković, *New J. Phys.* **21**, 053024 (2019).

[38] S. I. Mistakidis, A. G. Volosniev, N. T. Zinner, and P. Schmelcher, *Phys. Rev. A* **100**, 013619 (2019).

[39] V. Hakim, *Phys. Rev. E* **55**, 2835 (1997).

[40] G. Panochko and V. Pastukhov, *Ann. Phys.* **409**, 167933 (2019).

[41] A. Lamacraft, *Phys. Rev. B* **79**, 241105 (2009).

[42] M. Schechter, A. Kamenev, D. M. Gangardt, and A. Lamacraft, *Phys. Rev. Lett.* **108**, 207001 (2012).

[43] T. A. Yoğurt and M. T. Eiles, *Phys. Rev. A* **112**, 053306 (2025).

[44] J. Gunn and J. Gunn, *European Journal of Physics* **9**, 51 (1988).

[45] E. B. Kolomeisky, J. P. Straley, and R. M. Kalas, *Phys. Rev. A* **69**, 063401 (2004).

[46] V. A. Trofimov and N. V. Peskov, *Mathematical Modelling and Analysis* **14**, 109 (2009).

[47] S. Patankar, *Numerical Heat Transfer and Fluid Flow*, Series in computational methods in mechanics and thermal sciences (Taylor & Francis, 1980).

[48] A. M. Kamchatnov, A. Gammal, and R. A. Kraenkel, *Phys. Rev. A* **69**, 063605 (2004).

[49] M. A. Hoefer, M. J. Ablowitz, I. Coddington, E. A. Cornell, P. Engels, and V. Schweikhard, *Phys. Rev. A* **74**, 023623 (2006).